Optics Communications 402 (2017) 511–517

Contents lists available at ScienceDirect

Optics Communications

journal homepage: www.elsevier.com/locate/optcom

Performance analysis of all-optical XOR gate with photonic crystal semiconductor optical amplifier-assisted Mach–Zehnder interferometer at 160 Gb/s

Amer Kotb [a,b,*], Kyriakos E. Zoiros [c]

[a] Fayoum University, Faculty of Science, Department of Physics, Fayoum 63514, Egypt
[b] The Guo China-US Photonics Laboratory, Changchun Institute of Optics, Fine Mechanics, and Physics, Changchun 130033, China
[c] Lightwave Communications Research Group, Department of Electrical and Computer Engineering, School of Engineering, Democritus University of Thrace, Xanthi 67100, Greece

ARTICLE INFO

Keywords:
XOR gate
Photonic crystal
Semiconductor optical amplifier
Mach–Zehnder interferometer

ABSTRACT

The photonic crystal (PC) can be used to prohibit, confine, or control the propagation of light in a photonic band-gap. The performance of an ultrafast exclusive disjunction (XOR) gate-implemented with a photonic crystal semiconductor optical amplifier (PC-SOA)-assisted Mach–Zehnder interferometer (MZI) is numerically investigated and analyzed at a data rate of 160 Gb/s. The impact of the data signals and PC-SOA's critical parameters on the output quality factor (Q-factor) is examined and assessed. The simulation results demonstrate that the XOR gate which is based on the proposed scheme is capable of operating at the target data rate with logical correctness and high quality. This is achieved with better performance than when having conventional SOAs in the MZI, which justifies employing PC-SOAs as nonlinear elements.

1. Introduction

All-optical logic gates (AOLGs) are indispensable for the design, development, and implementation of circuits, subsystems, and networks in which digital information is handled while remaining in the optical form [1]. Especially, the exclusive disjunction (XOR) gate plays a catalytic role in this effort due to its involvement in the execution of numerous signal processing tasks both in fundamental and system-oriented level [2]. Given its significance, various technological approaches, which rely on optical nonlinearities, have been followed for its realization. Among them, SOAs offer the advantages of strong nonlinearity, compact size, and the potential for integration with other optoelectronics devices [3,4]. These features have made SOAs popular candidates for use as nonlinear elements in AOLGs. Thus, many SOA-based XOR gate schemes have been demonstrated, which have exploited SOA's nonlinear effects either in the SOA itself or in interferometric configurations [3–27].

On the other hand, the photonic crystal (PC) is a dielectric material whose dielectric constant is periodically varied in space. The lightwaves cannot propagate through the PC for some frequency range, which defines the photonic band-gap. The PC can be used to prohibit, confine, or control the propagation of light in a photonic band-gap. The advantages of the PC over other types of nonlinear structures are the reduction of absorption loss, suppression of undesirable nonlinear effects, low power consumption, and high power transmission. Thus, if these advantages were combined with those of SOA, AOLGs would clearly benefit from this combination. Indeed, the PC's slab waveguide for SOA was presented in [28], while AOLGs using PC quantum-dots SOAs have been modeled and designed [29,30].

The practical demonstration of PC-SOAs has opened the road for realizing ultra-high speed AOLGs by exploiting the former as nonlinear elements. In fact, PC-SOAs enable to considerably improve the performance of these logic modules [28–30]. In this novel study, the performance of the PC-SOA-based XOR gate is investigated by means of numerical simulation at a data rate of 160 Gb/s. The configuration used for this purpose is a Mach–Zehnder interferometer (MZI), which comprises of two symmetrically PC-SOAs placed in its arms. The MZI is very effective for achieving a variety of optical functions in a photonic optical waveguide circuit [3]. The impact of group index, radiation loss, confinement factor, pulse energy, injected current, pulse width, as well as PC-SOAs' carrier lifetime, saturation power, linewidth enhancement

* Corresponding author.
E-mail addresses: asm05@fayoum.edu.eg, kotb@phys.uconn.edu (A. Kotb), kzoiros@ee.duth.gr (K.E. Zoiros).

http://dx.doi.org/10.1016/j.optcom.2017.06.050
Received 7 April 2017; Received in revised form 13 June 2017; Accepted 14 June 2017
Available online 4 July 2017
0030-4018/

factor, length and thickness of PC-SOA's active region on the XOR gate output quality factor (Q-factor) is examined and assessed. Also, the impact of amplified spontaneous emission (ASE) on this metric has been included. ASE should be considered to obtain realistic and accurate results for the AOLGs. To our knowledge, there is no work in the literature that studies, through simulation analysis, the operation of PC-SOA-assisted MZI-based all-optical XOR gate with the ultimate goal to optimize its performance. The outcomes of this study suggest that the realization of the all-optical logic XOR gate is indeed feasible with the proposed PC-SOA-MZI scheme at 160 Gb/s, both with logical correctness and acceptable quality.

2. PC-SOA-MZI model

The operation of the PC-SOA-assisted MZI can be theoretically studied by means of a rate equation model [3,4]. By taking into account interband as well as intraband nonlinear effects, which include carrier depletion–recombination, carrier heating (CH), and spectral hole burning (SHB), the time-dependent gain for each PC-SOA has been derived as follows:

$$\frac{dh(t)}{dt} = \frac{h_0 - h(t)}{\tau_C} - \left(\frac{cR}{n_g}\right) h_{PC}[t] - \left(\exp\left[h(t) + h_{CH}(t) + h_{SHB}(t)\right] - 1\right) \frac{P(t)}{E_{sat}} \quad (1)$$

$$\frac{dh_{PC}(t)}{dt} = \left(\frac{LR}{\tau_c}\right)\left(h_0 - h_{PC}(t)\right) - \left(\frac{cR}{n_g}\right) h(t) \quad (2)$$

$$\frac{dh_{CH}(t)}{dt} = -\frac{h_{CH}(t)}{\tau_{CH}} - \frac{\varepsilon_{CH}}{\tau_{CH}}\left(\exp\left[h(t) + h_{CH}(t) + h_{SHB}(t)\right] - 1\right) P(t) \quad (3)$$

$$\frac{dh_{SHB}(t)}{dt} = -\frac{h_{SHB}(t)}{\tau_{SHB}} - \frac{\varepsilon_{SHB}}{\tau_{SHB}}\left(\exp\left[h(t) + h_{CH}(t) + h_{SHB}(t)\right] - 1\right) P(t) - \frac{dh(t)}{dt} - \frac{dh_{CH}(t)}{dt} \quad (4)$$

where functions 'h' represent the PC-SOA's gain integrated over its length for carrier depletion–recombination, PC, CH, and SHB, respectively. τ_c is the PC-SOA's carrier lifetime and $\exp[h_0] = G_0$ is the PC-SOA's unsaturated power gain, which is directly proportional to the PC-SOAs' injection current and active region length, L. $E_{sat} = P_{sat}\tau_c$ is the PC-SOA's saturation energy and P_{sat} is the PC-SOA's saturation power. $P(t)$ is the data power inserted into the PC-SOAs, which is linked to light intensity, $S(t)$, through $P(t) = \kappa S(t)$, where κ denotes the conversion factor from photon density to power. τ_{CH} and τ_{SHB} are the temperature relaxation rate and the carrier–carrier scattering rate, respectively. ε_{CH} and ε_{SHB} are the nonlinear gain suppression factors due to CH and SHB, respectively. c is the light velocity in a vacuum, n_g is the group index, L is the length, and R is the radiation loss of the active devices. Typically, $n_g = 3$, $L = 0.3$ cm, and $R = 30$ cm^{-1} for a standard SOA, while $n_g = 100$, $L = 10$ μm, and $R = 1500$ cm^{-1} for a PC-SOA [28].

The total gain $G(t)$ of the PC-SOA is then given by:

$$G(t) = \exp\left[h(t) + h_{CH}(t) + h_{SHB}(t)\right]. \quad (5)$$

The schematic diagram of PC-SOA's slab waveguide is illustrated in Fig. 1. The material used in this study is assumed to be GaInAsP. The common binary substrates are InP and GaAs. The PC-SOA is not suitable as a booster amplifier with high output power but is suitable as a preamplifier, optical gate, and for compensation of local loss with an output power from −10 to 0 dBm [28]. The PC-SOA is still very effective and attractive for constructing functional active photonic circuits.

The carrier density-induced phase change due to a PC-SOA is given by:

$$\Phi(t) = -0.5\left[\alpha h(t) + \alpha_{CH} h_{CH}(t)\right] \quad (6)$$

where α is the traditional linewidth enhancement factor associated with interband carrier dynamics, α_{CH} is the linewidth enhancement factor

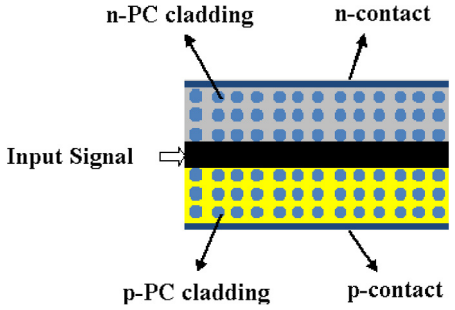

Fig. 1. Schematic diagram of PC-SOA's waveguide.

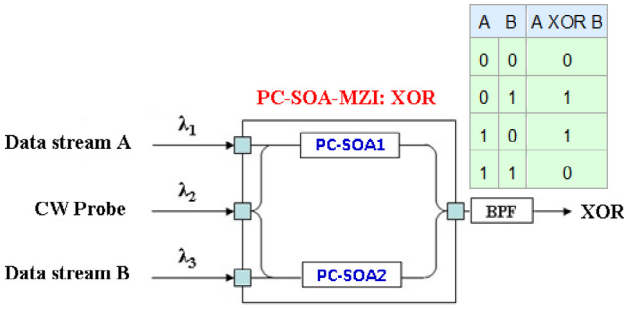

Fig. 2. Schematic diagram and truth table of XOR gate with PC-SOA-assisted MZI. BPF: Band-pass filter.

due to CH. The contribution governed by α_{SHB} is null because SHB produces asymmetrical spectral hole centered at the signal wavelength. In this case, the Kramers–Kronig integral becomes antisymmetric at the operating frequency and the Kramers–Kronig integral remains very small [31–35].

In this simulation, the data stream input pulses are assumed to be Gaussian-shaped whose power profile is described by the formula [3,4]:

$$P_{A,B}(t) = \sum_{n=-\infty}^{n=+\infty} a_{nA,B} \frac{2\sqrt{\ln(2)}E_0}{\sqrt{\pi}\tau_{FWHM}} \exp\left(-\frac{4\ln(2)(t-nT)^2}{\tau_{FWHM}^2}\right) \quad (7)$$

where $a_{nA,B}$ represents the nth pulse, which can take the logical value '1' or '0' with equal probability, in a pseudorandom binary sequence (PRBS) of length nT, where T is the single bit period and $n = 2^7 - 1$ is the PRBS's length. E_0 is the input pulse energy. τ_{FWHM} is the pulse width (full-width at half-maximum).

3. XOR modeling

3.1. Operation principle

The schematic diagram and the truth table of the XOR gate-implemented in PC-SOA-assisted MZI configuration is shown in Fig. 2. The XOR operation principle is as follows [3,4,27,31]: Two modulated data signals A (at wavelength λ_1) and B (at wavelength λ_3, which can be the same as the wavelength of data A) are separately injected into the two MZI's arms from ports 1 and 3. Concurrently, a continuous wave (CW) beam (at different wavelength λ_2) is injected from port 2. Then depending on their combination signals A and B will induce a phase shift on the split copies of the CW signal via cross-phase modulation (XPM) in the respective PC-SOAs. More specifically, for A = '0' and B = '0', the MZI remains balanced and there is no output or equivalently the logic outcome is '0'. When A = '1', B = '0', the copy of the CW signal traveling in the upper MZI arm together with signal A suffers through XPM a phase change versus its other split counterpart propagating in the lower MZI's arm. Thus, when these CW replicas recombine they interfere constructively, which results in output '1'. The same happens when A

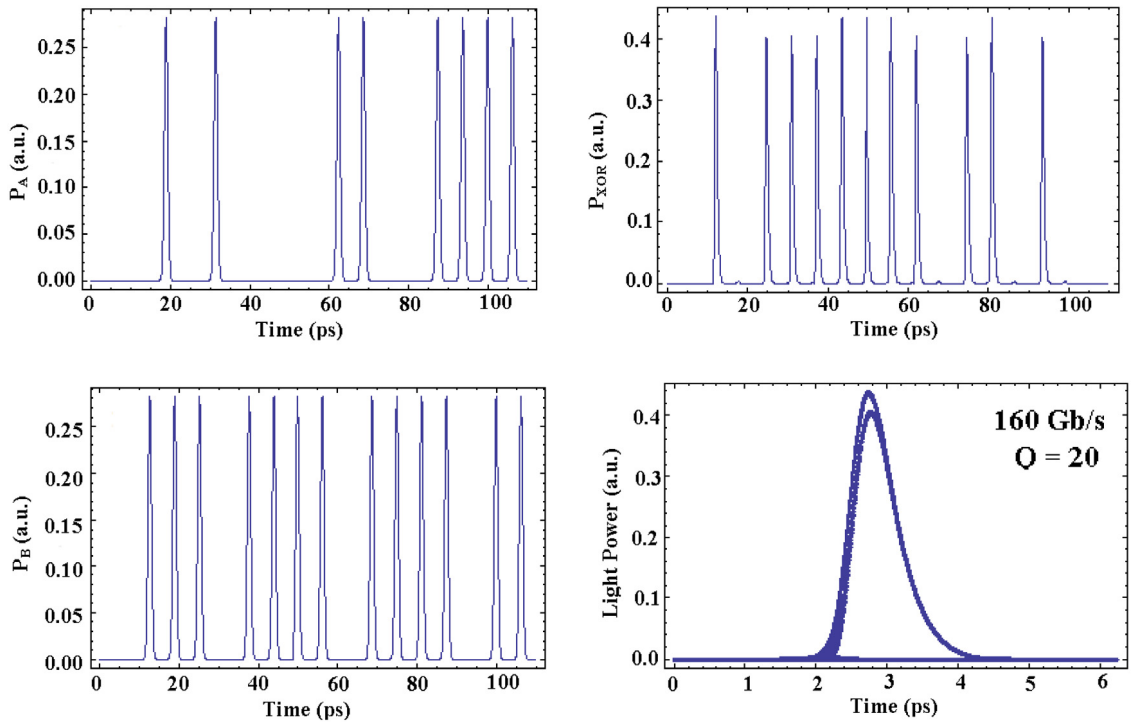

Fig. 3. Simulation results of PC-SOA-MZI for XOR operation. The achieved Q-value is 20 at a data rate of 160 Gb/s.

= '0' and B = '1'. However, when both A = '1' and B = '1', these CW constituents experience the same phase change, so they interfere destructively and the output is '0'. In this manner, the XOR operation is executed between the binary content of A and B according to the truth table of this Boolean function.

3.2. Simulation

The time-dependent output power of the XOR gate is described by the following basic interferometric equation [3,4]:

$$P_{XOR}(t) = 0.25P_{CW}\left\{G_1(t)+G_2(t)-2\sqrt{G_1(t)G_2(t)} \times \cos\left[\Phi_1(t)-\Phi_2(t)\right]\right\} \quad (8)$$

where P_{CW} stands for the power of the CW signal, while $G_{1,2}(t)$ and $\Phi_{1,2}(t)$ for the time-dependent gains and total phase shifts experienced by the copies of the CW signal inside PC-SOA1 and PC-SOA2, respectively. A set of operating parameters, which include the single pulse energy and width as well the PC-SOAs' injection current, carrier lifetime, linewidth enhancement factor, saturation power, group index, radiation loss, confinement factor, active region length and thickness and spontaneous emission factor critically affect the performance of the scheme at the target data rate. Thus in order to improve the performance of the proposed XOR gate, these parameters should be optimized. This can be done through numerical simulation and the computational program used to carry out this simulation has been prepared and run in Wolfram Mathematica®. This has been done by scanning each time one of the critical parameters while keeping the rest fixed to those values cited in Table 1.

To investigate the quality of XOR operation by simulation, the Q-value at the XOR output signal has been calculated. This metric is defined as $Q = (S_1 - S_0)/(\sigma_1 + \sigma_2)$ [3,4], where S_1, S_0 are the average intensities of the expected '1's and '0's and σ_1, σ_2 are the standard deviations of those intensities. Fig. 3 shows the simulation results of the binary outcome and eye diagram for the XOR gate for indicative patterns of data signals A and B. Owing to the use of the PC's slab waveguide [28–30], the achieved Q-factor is 20 at a data rate of 160 Gb/s, which is well over the critical limit and rather high compared to that previously reported in subject-related works [3–27].

Table 1
Calculation parameters.

Symbol	Definition	Value
E_0	Pulse energy	0.005 pJ
τ_c	PC-SOA's carrier lifetime	5 ps
τ_{FWHM}	Pulse width	1 ps
P_{sat}	Saturation power	30 mW
α	Linewidth enhancement factor	5
α_{CH}	Linewidth enhancement factor due to CH	1
α_{SHB}	Linewidth enhancement factor due to SHB processes	0
τ_{CH}	Temperature relaxation rate	0.3 ps
τ_{SHB}	Carrier–carrier scattering rate	0.1 ps
ε_{CH}	Nonlinear gain suppression factor due to CH	0.02 W^{-1}
ε_{SHB}	Nonlinear gain suppression factor due to SHB	0.02 W^{-1}
n_g	Group index	100
L	Length of active layer	10 μm
R	Radiation loss	1500 cm^{-1}
λ	Signal wavelength	1550 nm
Γ	Optical confinement factor	0.15

Fig. 4 shows the Q-factor as a function of PC-SOAs' group index and radiation loss for the XOR operation at 160 Gb/s. From this figure, it can be seen that the Q-factor is rather high within the entire group index scanned span. This is attributed to the higher signal gain enabled in this case [28], which in turn helps confine, and eventually smoothen, possible undesirable amplitude fluctuations of the XOR switched pulses around a less saturated level that does not impair the Q-factor [36]. On the other hand, it can also be observed that despite the higher radiation losses of PC-SOAs over standard SOAs, it is still possible to obtain a high Q-factor owing to the sufficient compensation of these losses by the large gain attained at a much lower bias current [28]. This could make a difference concerning the design, construction, and overall optimization of the respective active device.

The saturation energy (E_{sat}) of the amplifiers is given by [3]:

$$E_{sat} = \frac{h\omega_0\sigma_m}{a_N\Gamma} \quad (9)$$

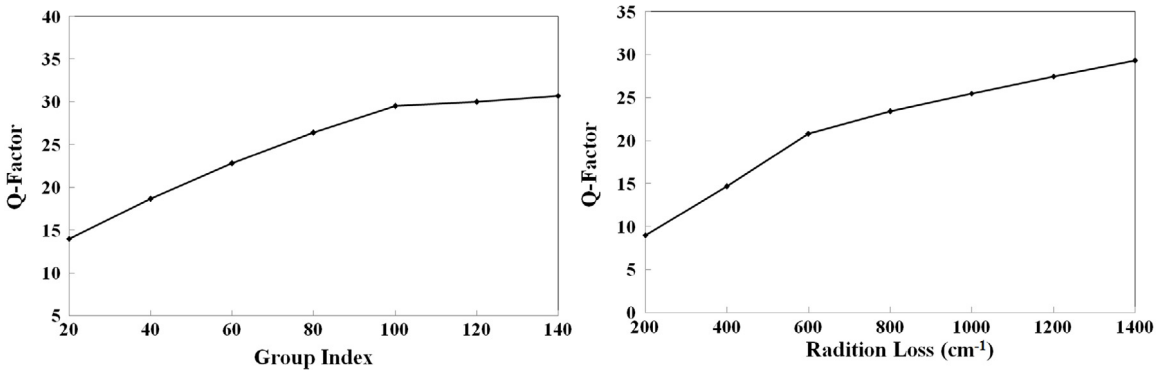

Fig. 4. Q-factor as a function of PC-SOAs' group index and radiation loss for XOR operation at 160 Gb/s.

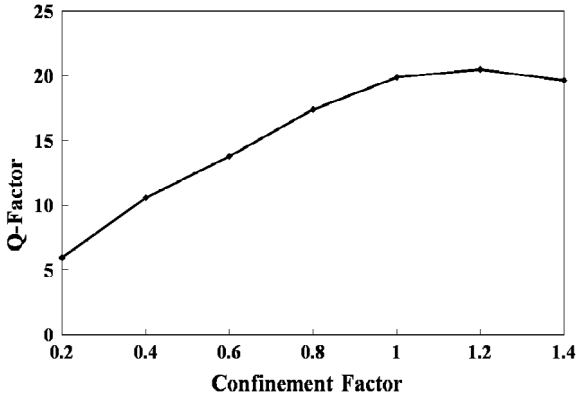

Fig. 5. Q-factor versus confinement factor for XOR operation at 160 Gb/s.

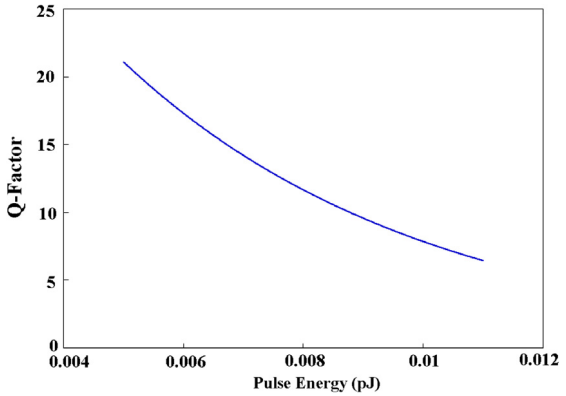

Fig. 6. Simulated Q-factor for different values of input single-pulse energies at 160 Gb/s.

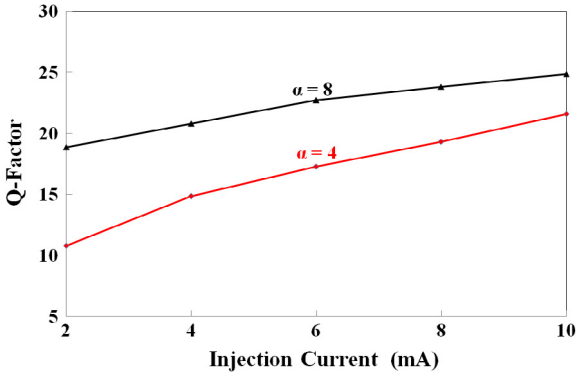

Fig. 7. Q-factor as a function of injection current for α-factors of 4 and 8.

where σ_m is the cross-section of the active region, i.e., $\sigma_m \cong wd$ (w and d are the width and thickness of the active layer). a_N is the differential gain, which equals 2×10^{-16} cm^{-3} for GaInAsP and Γ is the optical confinement factor. Fig. 5 shows that at low values of the PC-SOA's confinement factor the output signal is degraded and the Q-value is decreased. This happens because a decrease of this parameter affects analogously the unsaturated gain while having an opposite effect on E_{sat} [37]. As a result, it becomes more difficult to saturate the PC-SOAs at the proper level and accordingly induce the sufficient amount of differential phase shift in the MZI, which impairs achieving switching according to the Boolean function of the all-optical XOR gate.

To get further insight into the XOR gate performance, the Q-factor for different values of input single-pulse energies is shown in Fig. 6 at a data rate of 160 Gb/s. An increase of the input pulse energy causes a heavier saturation of the PC-SOAs, which leads to a decrease in the Q-factor. Still, the required switching energy is comparable to that of XOR gate implemented at 160 Gb/s with conventional SOA-MZI, which implies that even with PC-SOAs it is feasible to bring the input data pulses to the required amplitude level without the need to use complex and power consuming erbium-doped fiber amplifiers.

The number of free carriers increases with the external supply of more current into the PC-SOAs. This, in turn, leads to faster gain recovery time and hence enhanced PC-SOAs' dynamic response. Thus, as shown in Fig. 7, which has been obtained for two values of linewidth enhancement factor (4 and 8), the Q-factor is analogously affected. This fact is beneficial for the implementation of the scheme, since the PC-SOAs can be driven using less complex and power consuming electronic circuitry. In the standard SOAs, the amount of gain required for proper switching occurs at an injection current $I > 50$ mA, while it occurs at $I > 5$ mA in the PC-SOAs.

The calculated Q-factor as a function of the pulse width and the PC-SOAs' carrier lifetime is shown in Fig. 8. The Q-factor is rather sensitive to the input pulse width, as shown in Fig. 8(a). The Q-factor decreases when increasing the pulse width because, for a given peak power, pulses become more energetic, thereby causing stronger saturation of the PC-SOAs' gain which impairs the switching procedure and outcome. Nevertheless, an acceptable Q-factor can be obtained with pulses which are broad enough to relax the requirements on the optical sources needed to generate these pulses. On the other hand, the results in Fig. 8(b) show that the Q-factor also decreases as the carrier lifetime increases. Since the PC-SOAs' carrier lifetime determines the speed of gain and phase recovery in the active region, the Q-factor becomes higher for a shorter lifetime.

The PC-SOAs' gain is saturated when the input optical power is comparable to the saturation power (P_{sat}) [15]. Thus, the latter is a critical parameter for the performance of the XOR gate. The dependence

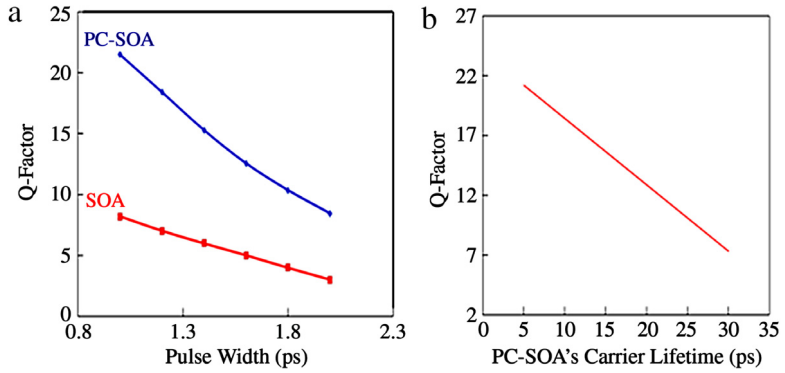

Fig. 8. (a) Calculated Q-factor as a function of pulse width; (b) dependence of calculated Q-factor on PC-SOAs' carrier lifetime for XOR operation.

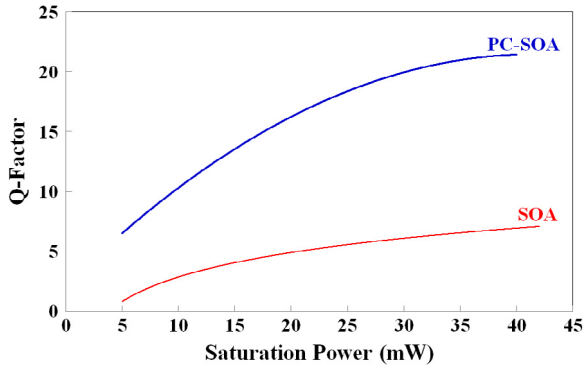

Fig. 9. Simulated Q-factor as a function of saturation power (P_{sat}) for PC-SOA and conventional SOA-based XOR operation.

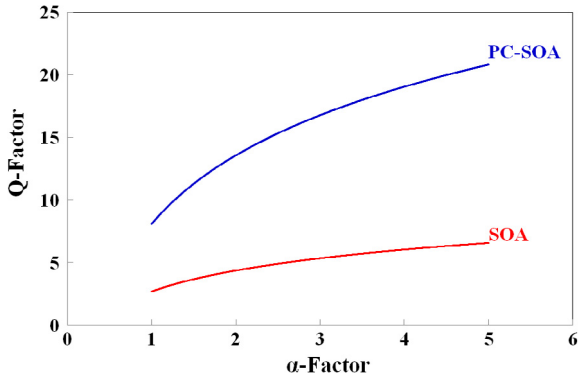

Fig. 10. Dependence of simulated Q-factor on linewidth enhancement factor (α-factor) for PC-SOA and conventional SOA-based XOR operation.

of the Q-factor on the saturation power is shown in Fig. 9 for PC-SOAs and conventional SOAs. It is seen that although the Q-factor rises in both cases, yet the inclination is more pronounced for the PC-SOAs than for the conventional SOAs. As a by-product, the Q-factor becomes acceptable across the whole scanned range of the examined parameter only for the PC-SOAs. Furthermore, if this was also going to happen for the conventional SOAs, it would require a much higher saturation power than for the PC-SOAs. From a power-wise standpoint, this implies that the switching operation can be achieved more efficiently for the PC-SOAs. Therefore, PC-SOAs are mostly suitable for use as nonlinear elements in an all-optical gate.

The linewidth enhancement factor (α-factor) depends on the relative position of the amplifier gain peak and the signal wavelengths. The simulated Q-factor as a function of α-factor for PC-SOAs and conventional SOAs is shown in Fig. 10. The Q-factor is ameliorated for larger α-factor because in this case, the incurred phase changes become more pronounced and hence the magnitude of the XOR signal (binary "1" values) is enhanced. In the ideal Gaussian energy distribution the gain spectrum is perfectly symmetric around the peak gain energy and $\alpha = 0$. But due to the variation of the carrier density and thermal effects, in practice, the α-factor is not zero. Because the integrated gain response (Eq. (1)) is more enhanced for the PC-SOAs than for the conventional SOAs, the necessary phase shift (Eq. (6)) can be incurred more efficiently in the former than in the latter case. Consequently, the Q-factor can be higher and more acceptable for PC-SOAs using a smaller alpha-factor compared to standard SOAs. Since the values of this parameter change depending on the operating conditions [38], this means that the latter can be relaxed, which may be desirable from a practical perspective.

Fig. 11(a) shows that the Q-factor increases for longer PC-SOAs driven at higher injection currents. A longer PC-SOA leads to increased carrier densities and subsequently exponential-like increase of the overall gain required for proper switching. Still, PC-SOAs can have a much lower length, such as 9 μm, which is an order of magnitude lower than conventional SOAs [28]. The optical gain region is also determined by the width of the PC-SOA's active region, which must favor acceleration of the gain recovery time and hence ultrafast operation of the all-optical gate incorporating these nonlinear elements. Thus, Fig. 11(b) shows that the Q-factor increases by making the PC-SOAs active region thicker. The findings of Fig. 11 suggest that the total size of the PC-SOAs is smaller than if conventional SOAs were used, which renders the scheme more compact and subsequently enhances its integration potential. Note that in the numerical extraction of Fig. 11(a) and (b) we have properly modified the injection current within the span defined in Fig. 7 so as to keep constant the current density when varying the PC-SOAs active region length and width [28], respectively. This is also implied in Fig. 11(b) so that the PC-SOAs confinement factor takes typical values for PC-SOAs [28] while its ratio versus the active region cross-section area is held constant and so does the PC-SOAs saturation energy [39] (see Eq. (9)).

The amplified spontaneous emission (ASE) is considered as noise, which degrades the SOA performance. If the spontaneous emission photons are emitted close to the direction of the signal photons, they will interact and cause both amplitude and phase fluctuations. The noise effect on the Q-factor is accounted for by adding numerically to the power of the XOR output pulses the ASE power, which is calculated using the following equation [31–33]:

$$P_{ASE} = N_{SP}\left(G_0 - 1\right) h\upsilon B_0 \tag{10}$$

where N_{sp} is the spontaneous emission factor, h is Planck's constant, and B_0 is the optical bandwidth at optical frequency υ. In using (10) it is assumed that ASE's noise does not affect the PC-SOAs' gain dynamics. This assumption is valid when the saturated optical gain is small [40], as it happens in our case where the PC-SOAs must operate in this saturation

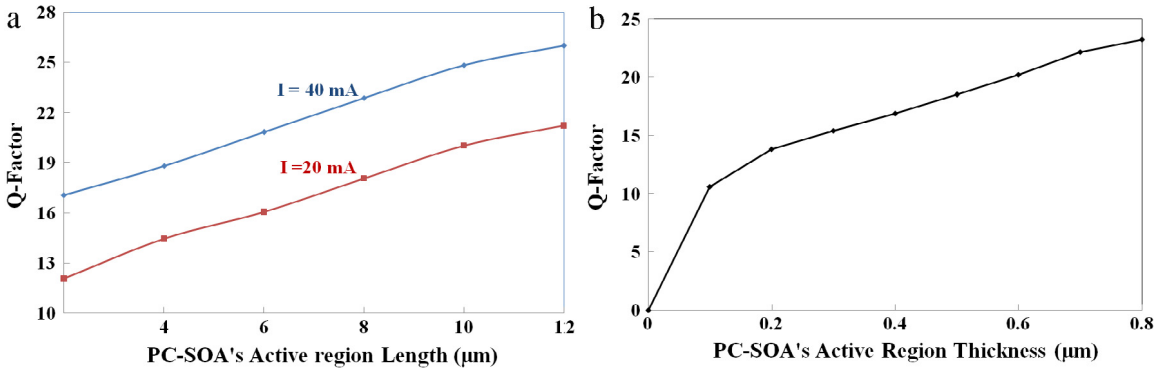

Fig. 11. Dependence of Q-factor on (a) length and (b) active region thickness of PC-SOA.

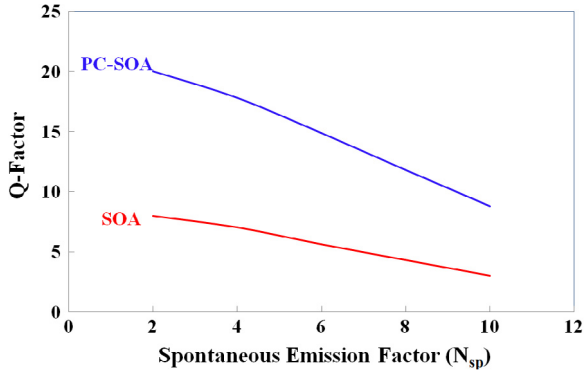

Fig. 12. Dependence of calculated Q-factor on spontaneous emission factor (N_{sp}) for PC-SOA and conventional SOA-based XOR operation.

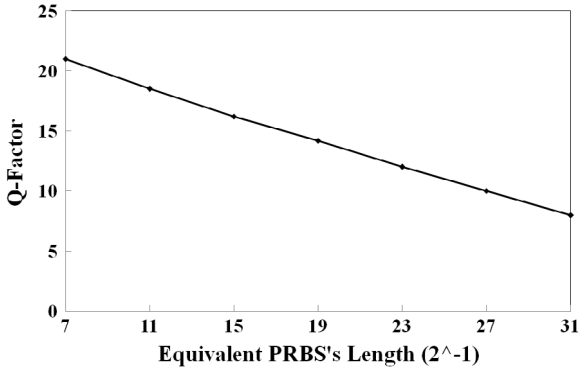

Fig. 13. Q-factor versus equivalent PRBS's length for PC-SOA-based XOR operation.

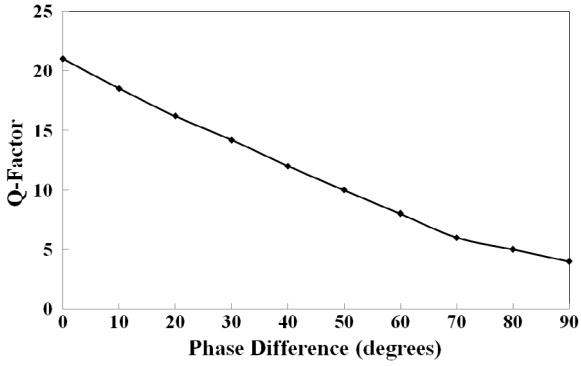

Fig. 14. Dependence of Q-factor on phase difference for PC-SOA-based XOR operation.

region in order to realize the target Boolean logic functionality. The Q-factor variation versus N_{sp} for PC-SOAs and conventional SOAs is shown in Fig. 12. This simulation is carried-out at a data speed of 160 Gb/s, $B_0 = 3$ nm, and $\lambda = 1550$ nm. Experimentally, the ASE is the easiest optical SOA characteristic to be measured. The impact of ASE is experimentally verified by adding wideband (few nm wide) optical unmodulated signal to the input data signal and measuring the Q-factor as a function of the intensity and bandwidth of this signal. The ASE adds a noise to the output level of bits '0' and '1'. Thus a larger ASE's noise increases the average intensity of the '0' level and hence reduces the Q-factor. Furthermore, it aggravates the pattern effect induced on the '1' and '0' levels, which, through the standard deviations (σ_1, σ_2), affects again negatively the Q-factor. Fig. 12 shows that the contribution of ASE affects less PC-SOA than conventional SOAs, since the Q-factor is acceptable and higher for the former than for the latter nonlinear elements. This can be an important advantage when exploiting the all-optical XOR gate in its target applications [2].

Fig. 13 shows that the ultrafast operation of the scheme is robust against different equivalent lengths [22] of the PRBS entering each control port. In fact, although the Q-factor is decreased due to the increased pattern-dependence, yet it remains acceptable, which is attributed to the much shorter carrier lifetime offered by PC-SOAs.

Fig. 14 investigates the impact of a sort of phase difference between the PC-SOA-MZI arms on the Q-factor. This may occur due to external factors, such as fluctuations in the ambient temperature, path length imbalance in the fiber-based MZI version or offset in the wavelength of the data signals [41]. These factors may impair the conditions for creating the required differential phase shift in the MZI, which however must properly be met in order to achieve switching according to the truth table of the considered gate. This extra phase is mathematically accounted for [42] by adding it to the cosine argument in Eq. (8), which gives the XOR gate output power. Then, Fig. 14 shows that the Q-factor and hence the performance of the logic scheme is fairly tolerant to such phase perturbations up to approximately 0.38π.

4. Conclusions

In conclusion, the operation of an ultrafast exclusive disjunction (XOR) gate has been simulated and its performance has been theoretically analyzed at a data speed of 160 Gb/s by using as switching module a photonic crystal semiconductor optical amplifier (PC-SOA)-assisted Mach–Zehnder interferometer (MZI). The investigation of the influence of the critical operating parameters on the Q-factor reveals that the latter can be as high as 20, which is well over the tolerable limit of this metric. The obtained results denote that it is feasible to employ PC-SOAs in a MZI for executing at ultrafast data rates fundamental Boolean logic functions entirely in the optical domain and this can be achieved with better performance than if conventional SOAs were

used instead. Therefore, PC-SOAs are very effective and attractive as nonlinear elements for constructing active photonic circuits based on them.

Acknowledgments

The author would like to thank the editor of the journal and anonymous referees.

References

[1] A. Bogoni, L. Potì, P. Ghelfi, M. Scaffardi, C. Porzi, F. Ponzini, G. Meloni, G. Berrettini, A. Malacarne, G. Prati, OTDM-based optical communications networks at 160 Gbit/s and beyond, Opt. Fiber Technol. 13 (2007) 1–12.
[2] E. Dimitriadou, K.E. Zoiros, All-optical XOR gate using single quantum-dot SOA and optical filter, J. Lightwave Technol. 31 (2013) 3813–3821.
[3] N.K. Dutta, Q. Wang, Semiconductor Optical Amplifiers, second ed., World Scientific Publishing Company, Singapore, 2013.
[4] A. Kotb, All-Optical Logic Gates using Semiconductor Optical Amplifier, LAMBERT Academic Publishing, Germany, 2012.
[5] T. Houbavlis, K.E. Zoiros, Ultrafast pattern-operated all-optical Boolean semiconductor optical amplifier-assisted Sagnac switch, Opt. Eng. 42 (2013) 3415–3419.
[6] C. Bintjas, M. Kalyvas, G. Theophilopoulos, T. Stathopoulos, H. Avramopoulous, L. Occhi, L. Schares, G. Guekos, S.R. Hansmann, R. Dall'Ara, 20 Gb/s all-optical XOR with UNI gate, IEEE Photonics Technol. Lett. 12 (2000) 834–838.
[7] T. Fjelde, D. Wolfson, A. Kloch, B. Dagens, A. Coquelin, I. Guillemot, F. Gaborit, F. Poingt, M. Renaud, A. Coquelin, I. Guillemot, Demonstration of 20 Gb/s all-optical logic XOR in integrated SOA-based interferometric wavelength converter, Electron. Lett. 36 (2000) 1863–1867.
[8] H. Chen, G. Zhu, J. Jaques, A.B. Leuthold, . Piccirilli, N.K. Dutta, All-optical logic XOR using a differential scheme and Mach–Zehnder interferometer, Electron. Lett. 38 (2002) 1271–1276.
[9] F. Ginovart, J.C. Simon, Gain dynamics study of a semiconductor optical amplifier, Opt. A.: Pure Appl. Opt. 4 (2002) 283–288.
[10] J.H. Kim, Y.M. Jhon, Y.T. Byun, S. Lee, D.H. Woo, S.H. Kim, All-optical XOR gate using semiconductor optical amplifiers without additional input beam, IEEE Photonics Technol. Lett. 14 (2002) 1436–1439.
[11] K. Chan, C. Chan, L. Chen, F. Tong, Demonstration of 20-Gbit/s all-optical XOR gate by four-wave mixing in semiconductor optical amplifier with RZ-DPSK modulated inputs, IEEE Photonics Technol. Lett. 16 (2004) 897–901.
[12] Z. Li, Y. Liu, S. Zhang, H. Ju, H. de-Waardt, G.D. Khoe, S. Dorren, D. Lenstra, All-optical logic gates using semiconductor optical amplifiers assisted by optical filter, Electron. Lett. 41 (2005) 1397–1400.
[13] Z. Li, G. Li, Ultrahigh-speed reconfigurable logic gates based on four-wave mixing in a semiconductor optical amplifier, IEEE Photonics Technol. Lett. 18 (2006) 1341–1345.
[14] S. Ma, Z. Chen, N.K. Dutta, All-optical logic gates based on two-photon absorption in semiconductor optical amplifiers, Opt. Commun. 282 (2009) 4508–4514.
[15] Q. Wang, G. Zhu, H. Chen, J. Jaques, J. Leuthold, A.B. Piccirilli, N.K. Dutta, Study of all-optical XOR using Mach–Zehnder Interferometer and differential scheme, IEEE J. Quantum Electron. 40 (2004) 703–709.
[16] S. Randel, A.M. de Melo, K. Petermann, V. Marembert, C. Schubert, Novel scheme for ultrafast all-optical XOR operation, Lightwave Technol. 22 (2004) 2808–2814.
[17] J.Y. Kim, J.M. Kang, T.Y. Kim, S.K. Han, 10 Gbits all-optical composite logic gates with XOR, NOR, OR and NAND functions using SOA-MZI structures, Electron. Lett. 42 (2006) 303–307.
[18] J.M. Martínez, F. Ramos, J. Martí, 10 Gb/s reconfigurable optical logic gate using a single hybrid-integrated SOA-MZI. Fib. and Integrat, Opt. 27 (2008) 15–20.
[19] R. Gutiérrez-Castrejón, Turbo-switched Mach–Zehnder interferometer performance as all-optical signal processing element at 160 Gb/s, Opt. Commun. 282 (2009) 4345–4350.
[20] S. Singh, Lovkesh, Ultrahigh speed optical signal processing logic based on an SOA-MZI, IEEE J. Sel. Top. Quantum Electron. 18 (2012) 970–975.
[21] R.P. Webb, X. Yang, R.J. Manning, R. Giller, All-optical 40 Gbit/s XOR gate with dual ultrafast nonlinear Interferometer, Electron. Lett. 41 (2005) 1396–1400.
[22] K.E. Zoiros, T. Siarkos, D. Nastou, On the feasibility of full pattern-operated all-optical XOR gate with single semiconductor optical amplifier-based ultrafast nonlinear interferometer, Opt. Commun. 282 (2009) 2729–2734.
[23] K.E. Zoiros, C. Demertzis, On the speed extension of semiconductor optical amplifier-based ultrafast nonlinear interferometer in dual rail switching mode using a cascaded optical delay interferometer, Opt. Laser Technol. 43 (2011) 1190–1195.
[24] M. Zhang, L. Wang, P. Ye, All-optical XOR logic gates: Technologies and experiment demonstrations, IEEE Commun. Mag. 43 (2005) S19–S23.
[25] H. Sun, Q. Wang, H. Dong, Z. Chen, N.K. Dutta, J. Jaques, A.B. Piccirilli, All-optical logic XOR gate at 80 Gb/s using SOA-MZI-DI, IEEE J. Quantum Electron. 42 (2006) 747–751.
[26] I. Kang, M. Rasras, L. Buhl, M. Dinu, S. Cabot, M. Cappuzzo, L.T. Gomez, Y.F. Chen, S.S. Patel, N. Dutta, A. Piccirilli, J. Jaques, C.R. Giles, All-optical XOR and XNOR operations at 86.4 Gb/s using a pair of semiconductor optical amplifier Mach–Zehnder interferometers, Opt. Express 17 (2009) 19062–19066.
[27] A. Kotb, K.E. Zoiros, Performance of all-optical XOR gate based on two-photon absorption in semiconductor optical amplifier-assisted Mach–Zehnder interferometer with effect of amplified spontaneous emission, Opt. Quantum Electron. 46 (2014) 935–941.
[28] E. Mizuta, H. Watanabe, T. Baba, All semiconductor low-Δ photonic crystal waveguide for semiconductor optical amplifier, Japan. J. Appl. Phys. 45 (2006) 6116–6120.
[29] H. Taleb, K. Abedi, Modeling and design of photonic crystal quantum-dot semiconductor optical amplifiers, IEEE Trans. Electron Devices 61 (2014) 2419–2423.
[30] H. Taleb, K. Abedi, Design of a novel low power all-optical NOR gate using photonic crystal quantum-dot semiconductor optical amplifiers, Opt. Lett. 39 (2014) 6237–6241.
[31] A. Kotb, S. Ma, Z. Chen, N.K. Dutta, G. Said, Effect of amplified spontaneous emission on semiconductor optical amplifier based all-optical logic, Opt. Commun. 284 (2011) 5798–5803.
[32] A. Kotb, Simulation of all-optical logic NOR gate based on two-photon absorption with semiconductor optical amplifier-assisted Mach–Zehnder interferometer with the effect of amplified spontaneous emission, Korean Phys. Soc. 66 (2015) 1593–1598.
[33] A. Kotb, K.E. Zoiros, On the design of all-optical gates based on quantum-dot semiconductor optical amplifier with effect of amplified spontaneous emission, Opt. Quantum Electron. 46 (2014) 977–982.
[34] A. Kotb, Simulation of high-quality factor all-optical logic gates based on quantum-dot semiconductor optical amplifier at 1 Tb/s, Optik 126 (2016) 320–325.
[35] A. Kotb, Modeling of high-quality factor XNOR gate using quantum-dot semiconductor optical amplifiers at 1 Tb/s, Braz. J. Phys. 45 (2015) 288–295.
[36] K.E. Zoiros, J. Vardakas, T. Houbavlis, M. Moyssidis, Investigation of SOA-assisted Sagnac recirculating shift register switching characteristics, Optik 116 (2005) 527–541.
[37] R. Bonk, T. Vallaitis, J. Guetlein, C. Meuer, H. Schmeckebier, D. Bimberg, C. Koos, W. Freude, J. Leuthold, The input power dynamic range of a semiconductor optical amplifier and its relevance for access network applications, IEEE Photonics J. 3 (2011) 1039–1053.
[38] L. Schares, C. Schubert, C. Schmidt, H.G. Weber, L. Occhi, L. Guekos, Phase dynamics of semiconductor optical amplifiers at 10 to 40 GHz, IEEE J. Quantum Electron. 39 (2003) 1394–1408.
[39] R. Giller, R.J. Manning, G. Talli, R.P. Webb, Analysis of the dimensional dependence of semiconductor optical amplifier recovery speeds, Opt. Express 15 (2007) 1773–1782.
[40] J.L. Wei, X.L. Yang, R.P. Giddings, J.M. Tang, Colourless adaptively modulated optical OFDM transmitters using SOAs as intensity modulators, Opt. Express 17 (2009) 9012–9027.
[41] C.S. Wong, H.K. Tsang, Filtering directly modulated laser diode pulses with a Mach–Zehnder optical delay interferometer, Electron. Lett. 40 (2004) 938–940.
[42] J. Leuthold, P.A. Besse, J. Eckner, E. Gamper, M. Dulk, H. Melchior, All-optical space switches with gain and principally ideal extinction ratios, IEEE J. Quantum Electron. 34 (1998) 622–633.